Brian G. Drew,[1] Vicente Ribas,[1] Jamie A. Le,[1] Darren C. Henstridge,[2] Jennifer Phun,[1] Zhenqi Zhou,[1] Teo Soleymani,[1] Pedram Daraei,[1] Daniel Sitz,[1] Laurent Vergnes,[3] Jonathan Wanagat,[4] Karen Reue,[3] Mark A. Febbraio,[2] and Andrea L. Hevener[1]

HSP72 Is a Mitochondrial Stress Sensor Critical for Parkin Action, Oxidative Metabolism, and Insulin Sensitivity in Skeletal Muscle

Diabetes 2014;63:1488–1505 | DOI: 10.2337/db13-0665

METABOLISM

Increased heat shock protein (HSP) 72 expression in skeletal muscle prevents obesity and glucose intolerance in mice, although the underlying mechanisms of this observation are largely unresolved. Herein we show that HSP72 is a critical regulator of stress-induced mitochondrial triage signaling since Parkin, an E3 ubiquitin ligase known to regulate mitophagy, was unable to ubiquitinate and control its own protein expression or that of its central target mitofusin (Mfn) in the absence of HSP72. In wild-type cells, we show that HSP72 rapidly translocates to depolarized mitochondria prior to Parkin recruitment and immunoprecipitates with both Parkin and Mfn2 only after specific mitochondrial insult. In HSP72 knockout mice, impaired Parkin action was associated with retention of enlarged, dysmorphic mitochondria and paralleled by reduced muscle respiratory capacity, lipid accumulation, and muscle insulin resistance. Reduced oxygen consumption and impaired insulin action were recapitulated in Parkin-null myotubes, confirming a role for the HSP72-Parkin axis in the regulation of muscle insulin sensitivity. These data suggest that strategies to maintain HSP72 may provide therapeutic benefit to enhance mitochondrial quality and insulin action to ameliorate complications associated with metabolic diseases, including type 2 diabetes.

Cellular stress resistance against inflammatory and metabolic insult is critical for disease prevention and longevity (1–3). The heat shock response is an evolutionarily conserved defense system engaged during stress (e.g., thermal stress, ultraviolet exposure, and nutrient oversupply) so as to maintain cellular homeostasis. Heat shock factor (HSF) 1 is a key transcription factor regulating the induction of a number of heat shock proteins (HSPs), each identified by molecular mass, e.g., HSP27, HSP40, HSP60, HSP72, and HSP90. We have focused our efforts studying HSP72, the isoform most highly induced during cellular stress and with chronic endurance exercise (4). Importantly, basal HSP72 levels and induction response to cellular stress are diminished in muscle from obese and type 2 diabetic patients (5,6).

To improve our understanding of the relationship between HSP72 expression and disease susceptibility, we experimentally elevated HSP72 specifically in muscle or globally in mice by genetic or pharmacologic means and found that this conferred protection against diet- and leptin deficiency–induced obesity and insulin resistance (6). We hypothesized that the protective effect of HSP72 to maintain insulin action may be due in part to prevention of proinflammatory signaling via c-jun N-terminal kinase (6). In addition to the potential direct effects of HSP72 in blocking inflammation, oxidative metabolism was elevated in muscle overexpressing HSP72 (6), and this was associated with reduced adipose tissue mass and increased circulating adiponectin levels, factors also associated with

[1]David Geffen School of Medicine, Department of Medicine, Division of Endocrinology, Diabetes and Hypertension, University of California, Los Angeles, Los Angeles, CA
[2]Baker IDI Heart and Diabetes Institute, Melbourne, Victoria, Australia
[3]David Geffen School of Medicine, Department of Human Genetics, University of California, Los Angeles, Los Angeles, CA
[4]David Geffen School of Medicine, Department of Medicine, Division of Geriatrics, University of California, Los Angeles, Los Angeles, CA

Corresponding author: Andrea L. Hevener, ahevener@mednet.ucla.edu.

Received 25 April 2013 and accepted 23 December 2013.

This article contains Supplementary Data online at http://diabetes.diabetesjournals.org/lookup/suppl/doi:10.2337/db13-0665/-/DC1.

preservation of insulin action in the context of overnutrition (6). Although we have provided strong evidence of a relationship between HSP72 expression and insulin action, it has remained unclear whether reduced HSP72 levels are causal for insulin resistance and, if so, by what mechanism(s).

For the first time, we show that HSP72 translocates to depolarized mitochondria and is critical for regulating functionality of the E3 ubiquitin ligase Parkin, a protein involved in mitochondrial quality control (7). Herein we show that mice lacking HSP72 display glucose intolerance and skeletal muscle insulin resistance. Moreover, Parkin-null myotubes recapitulated the impairment in oxygen consumption and insulin action observed with a Parkin loss-of-function phenotype in HSP72 knockout (KO) mice. Thus our findings suggest a novel link between diminished HSP72 levels and Parkin inactivation that precipitate derangements in skeletal muscle mitochondrial function and insulin action.

RESEARCH DESIGN AND METHODS

Animals

Male wild-type (WT) and HSP72-KO (global null mutation of Hspa1a/Hspa1b genes; Mutant Mouse Regional Resource Center Repository) were obtained at 8 weeks of age. WT and KO animals were confirmed to be of pure C57BL/6 background (The Jackson Laboratory). Ten cohorts of HSP72-KO mice bred at the University of California, Los Angeles (UCLA), were used for in vivo and ex vivo investigation. Although substrain analysis of inbred cohorts revealed a 16–86% C57BL/6 J:N, specific end points, i.e., Parkin protein and insulin action, were similarly and consistently altered between the genotypes of multiple cohorts of animals. Subsequently, KO mice were backcrossed to WT C57BL/6J or mice with muscle-specific transgenic overexpression of HSP72 ($mHSP72^{Tg}$) (6) to obtain WT, HSP72 homozygous and heterozygous littermates with and without the muscle-specific transgene. Male Parkin-null and WT mice were obtained from The Jackson Laboratory at 10 weeks of age, and muscle was harvested at 12 weeks to obtain primary myotubes. All procedures were performed in accordance with the Guide for Care and Use of Laboratory Animals of the National Institutes of Health and were approved by the Animal Subjects Committee of UCLA. At age 8–10 weeks, WT and HSP72-KO animals were divided into two groups: basal versus insulin-stimulated. Animals were studied in the 6-h fasted condition unless otherwise specified as fed or starved (24 h). Ages in which the animals were studied are indicated in Table 1 and in the figure legends.

Heat and Leupeptin Treatment Studies

Animals were exposed to one acute heat treatment to assess the induction of HSP72 in WT and HSP72-KO mice. Prior to heat treatment, mice were anesthetized with a mouse cocktail of ketamine, xylazine, and acepromazine maleate as described previously (8). While unconscious, a rectal thermometer was inserted, and mice were placed in a ventilated plastic container wrapped with a heating blanket (6). During heat treatment, body temperature was allowed to rise gradually (10–15 min) to 41.5°C and was maintained at this temperature for a total of 15 min. Animals were euthanized and tissues harvested 30 min after treatment.

To assess whether Parkin protein is degraded by the lysosome under basal conditions, 6-h fasted WT mice were treated for 1 h with leupeptin (L2884, Sigma-Aldrich; 40 mg/kg; intraperitoneal injection) to inhibit lysosomal proteases. Quadriceps muscle was harvested for Parkin and LC3B immunoblot analyses.

Circulating Factors, Glucose Tolerance, and Ambulatory Movement

Blood was drawn from 6-h fasted 8-, 20-, 28-week-old mice and analyzed for circulating factors: insulin, leptin, resistin (Multiplex, Millipore), and adiponectin (radioimmunoassay; Millipore). Intraperitoneal glucose tolerance tests (GTTs; 1 g/kg dextrose) were performed on 6-h fasted mice as previously described (8,9). In a separate cohort of animals, mice were acclimated to the metabolic chambers (Columbus Instruments) over the first 24 h, and ambulatory movement was recorded over the subsequent 48 h.

Hyperinsulinemic-Euglycemic Clamp Studies

At 28 weeks of age, dual catheters were surgically placed in the right jugular vein, and glucose clamp studies were performed 3 days postsurgery as previously described (8–10).

AMP-Activated Protein Kinase Activity

Muscle lysates were incubated with AMP-activated protein kinase (AMPK) α1- and α2-specific antibody-bound protein A agarose beads for 2 h. Sample immunocomplexes were washed and enzyme activity determined in the presence of 200 mmol/L AMP using SAMS peptide as described previously (11).

Muscle Fatty Acid Oxidation and Esterification

Fatty acid oxidation and esterification assays were performed on isolated soleus muscle as previously described (12).

Primary HSP72-KO Skeletal Muscle Cells

At 8–12 weeks of age, primary skeletal muscle myoblasts were isolated from WT, HSP72-KO, and Parkin-KO mice as previously described (13). Myoblasts were cultured to confluence then differentiated to myotubes in Dulbecco's modified Eagle's medium (DMEM)/5% horse serum for 5–7 days before experimentation.

Plasmids, Cloning, and Transfections

Cloning was performed using Gateway technology (Invitrogen). The mouse *hspa1b* open reading frame (ORF) entry clone was obtained from Open Biosystems (Thermo Scientific). HSP72-GFP and HSP72-pAD were generated by shuttling the *hspa1b*-ORF into pcDNA-DEST47 and

Table 1—Metabolic parameters and circulating factors

	HSP72-WT	HSP72-KO	*P* value
Basal (*n*)	20	16	
Clamp (*n*)	7	8	
Age (weeks)	8–28	8–28	
Body weight (g)			
8 weeks	23.6 ± 0.3	22.4 ± 0.2	0.12
20 weeks	29 ± 0.75	28 ± 0.59	0.9
28 weeks	29 ± 0.2	33 ± 0.4	0.01
28 weeks (clamped, weight matched)	31 ± 0.5	33 ± 1.0	0.5
Ambulatory movement (beam breaks/h)			
Horizontal	861 ± 95	916 ± 108	0.73
Vertical	350 ± 23	402 ± 53	0.46
Gonadal fat, 28 weeks (g)	0.41 ± 0.04	0.62 ± 0.04	0.03
Liver weight, 28 weeks (g)	1.1 ± 0.03	1.1 ± 0.05	0.51
Heart weight, 28 weeks (g)	0.139 ± 0.005	0.146 ± 0.009	0.48
Fasting blood glucose (mg/dL)	143 ± 4	130 ± 4	0.08
Clamp blood glucose (mg/dL)	131 ± 2	128 ± 4	0.57
Glucose infusion rate ($mg \cdot kg^{-1} \cdot min^{-1}$)	49 ± 2	33 ± 4.5	0.007
Fasting insulin (ng/mL)			
8 weeks	0.30 ± 0.05	0.30 ± 0.05	0.98
20 weeks	0.21 ± 0.08	0.50 ± 0.04	0.004
28 weeks	0.35 ± 0.02	0.62 ± 0.06	0.04
GTT insulin, 15 min (ng/mL)	1.35 ± 0.13	1.60 ± 0.40	0.64
Adiponectin, 28 weeks (μg/mL)	21 ± 1	8 ± 0.05	0.001
Leptin (ng/mL)			
8 weeks	0.56 ± 0.05	1.2 ± 0.07	0.006
20 weeks	1.37 ± 0.07	3.2 ± 0.39	0.03
28 weeks	1.34 ± 0.09	4.7 ± 0.28	0.0001
Resistin (ng/mL)			
8 weeks	0.39 ± 0.02	0.66 ± 0.06	0.06
20 weeks	0.46 ± 0.01	0.51 ± 0.02	0.03
28 weeks	0.29 ± 0.08	0.7 ± 0.02	0.0004

Data are presented as means ± SEM.

pAd/CMV/V5-DEST, respectively, using LR Clonase Enzyme Mix II as per manufacturer's instructions (Invitrogen). Parkin YFP (Addgene plasmid #23955), pDsRed2-mito, and mitofusin (Mfn) 2 plasmids were kind gifts from Antonio Zorzano (IRB Barcelona, Spain). HA Parkin and V5 Mfn2 entry clones were generated by BP-cloning (Gateway, Invitrogen) the ORF into pDONR221 using Parkin YFP and Mfn2 plasmids as templates, respectively. Inserts were then shuttled into custom Gateway N-Term HA- and V5-plasmids, respectively, using LR Clonase as described above. All positive clones were confirmed and sequenced for accuracy. Transfections were performed using Lipofectamine 2000 and PLUS reagent according to the manufacturer's instructions (Invitrogen).

Cell Culture and Treatments

HEK293A cells (ATCC) and Neuro2A (N2a; a gift from Douglas Black, UCLA) cells were maintained in DMEM containing 10% FBS and penicillin/streptomycin at 5% CO_2 and 37°C. C2C12 myoblasts (ATCC) were maintained and proliferated in DMEM/10% FBS and differentiated in DMEM/2% horse serum. Cell treatments were performed as follows, unless otherwise stated: MG132 (Sigma; cell permeable proteasomal inhibitor used to reduce the degradation of ubiquitin-conjugated proteins) at 20 μmol/L for 4 h, carbonyl cyanide *m*-chlorophenyl hydrazone (Sigma; CCCP was used to inhibit oxidative phosphorylation by collapsing the mitochondrial proton gradient) at 20 μmol for 4 h, bafilomycin A1 (Baf; Sigma; a selective inhibitor of vacuolar H^+-ATPases and thought to inhibit autophagy by blocking autophagosome–lysosome fusion and lysosomal degradation) at 25 nmol/L for 4 h, rotenone (specific inhibitor of electron transfer from iron–sulfur centers in mitochondrial complex I to ubiquinone) at 2 μmol/L for 4 h, antimycin (binds cytochrome c reductase inhibiting the oxidation of ubiquinol disrupting the proton gradient and ATP production) 40 μmol/L for 4 h, and starvation (Hanks' balanced salt solution: PBS 1:1 plus 1% horse serum) for 4 h. Imatinib (STI-571), a tyrosine kinase inhibitor prescribed in the treatment of multiple cancers,

was used at 10 μmol/L for 24 h to inhibit cABL from phosphorylating Parkin and altering its activity in HEK293A cells (14). Cellular heat shock was performed by placing cells at 42°C for 6 h with a 2-h recovery at 37°C prior to harvest as previously described (6).

Insulin-Stimulated 2-Deoxyglucose Uptake Into Myocytes

Cultured skeletal muscle cell glucose uptake was performed in 12-well culture plates using the 2-deoxyglucose method described previously (10).

Mitochondrial Respiration in Cultured Muscle Cells

Mitochondrial respiration (oxygen consumption) in cultured skeletal muscle cells was measured using an XF24 Extracellular Flux Analyzer (Seahorse Biosciences). Briefly, cells were plated to confluence (24-well plates) and differentiated as described above. Measurements of oxygen consumption were made continuously (every 10 s) while cells were sequentially treated with oligomycin (ATP synthase inhibitor), FCCP (an uncoupling agent), and rotenone/myxothiazol (inhibitors of complex I/III of the electron transport chain).

Fatty Acid Oxidation and Esterification in Cultured Muscle Cells

Fatty acid oxidation and esterification in cultured skeletal muscle myotubes were performed in six-well culture plates, as adapted from the method previously described (10).

Ex Vivo Soleus Muscle Strip Glucose Uptake

Whole muscle ex vivo glucose uptake was assessed using 2-deoxyglucose, with minor changes to that described previously (10,15).

Confocal Microscopy

Cells were plated on glass coverslips and cultured as described above. Following treatments, cells were washed and fixed in 4% phosphate-buffered formalin then mounted in VectaShield containing DAPI (Vector Laboratories) and sealed before being visualized on a Leica TCS-SP2 AOBS confocal microscope. Colocalization studies were assessed by ImageJ using the JACoP colocalization plugin (16).

Mitochondria Isolations

Mitochondria were isolated from WT and HSP72-KO primary myotubes and from HEK293A cells using two different methods. Mitochondria were isolated using a Dounce homogenizer and the Mitochondria Isolation Kit for Cultured Cells according to the manufacturer's instructions (Pierce Thermo Scientific) or by sucrose density method (17). Briefly, cells in 10 cm dishes were washed in ice-cold PBS, drained, and then scraped from plates in 8 mL ice-cold isolation buffer. Cells were disrupted with a Dounce homogenizer (10 × 20 s strokes), and cell debris were pelleted at 1,800*g* for 10 min at 4°C. Mitochondria in the supernatant were then pelleted at 7,000*g* for 10 min at 4°C and washed twice in isolation buffer before being solubilized in radioimmunoprecipitation assay (RIPA) buffer.

Adenoviral Overexpression in Cultured Skeletal Muscle

Adenoviral constructs/plasmids containing HSP72 (Hspa1b) were generated as described above. Live virus particles were produced in HEK293A cells using the ViraPower Adenoviral Expression System (Invitrogen). High titer virus was then used in a dose-dependent manner (0, 10, and 50 multiplicity of infection) to determine successful and optimal expression in primary myotubes before performing final experiments.

Lentiviral-Mediated Short Hairpin RNA Stable Knockdown

Lentiviral particles (Mission Transduction Particles; 10130816MN) expressing short hairpin RNAs (shRNAs) against Hspa1b (NM_010478) and a scrambled shRNA were purchased from Sigma-Aldrich. C2C12 cells were seeded at 20,000 cells in a six-well plate and exposed to virus particles for 24 h, after which virus was removed and cells were allowed to grow to ~80% confluence in normal growth media. Following this, cells were reseeded into a 10 cm dish, allowed to proliferate prior to selection over a 2-week period in sequential doses (1–10 μg/mL) of Puromycin (Enzo LifeSciences). After selection, cells were maintained in normal growth media, and successful knockdown (KD) of HSP72 was determined by both quantitative PCR (qPCR) and immunoblotting following heat shock.

Soluble and Insoluble Muscle Fractionation

Soluble and insoluble fractions of proteins were isolated as previously described (18).

Electron Microscopy

Dissected tissues were harvested and immediately immersed in 2% glutaraldehyde in PBS for 2 h at room temperature and then at 4°C overnight. Fixed tissues were washed and postfixed in a solution of 1% OsO_4 for 2 h. Tissues were dehydrated, embedded in pure epon 812, and cured (60°C for 48 h). Muscle longitudinal sections of 60 nm thickness were cut using an ultramicrotome (RMC MTX). The sections were double stained in aqueous solutions of 8% uranyl acetate for 25 min at 60°C and lead citrate for 3 min at room temperature. Thin sections were subsequently examined with a 100CX JEOL electron microscope.

Reactive Oxygen Species Measurements by Fluorescence Analysis

C2C12 myocytes were washed and incubated in low-glucose DMEM at 37°C, 5% CO_2 in the dark with 25 μmol/L of Carboxy-H_2DCF-DA (Molecular Probes, Invitrogen), washed with PBS and incubated 15 min with 5 μmol/L of MitoSOX, washed and quickly trypsinized, pelleted, and retained on ice. Cells were resuspended in fluorescence-activated cell sorter buffer (PBS 3% BSA) with DAPI (25 μg/mL) and analyzed immediately by flow cytometry on a LSRII (Becton Dickinson) with FlowJo software (Treestar Inc.). Unstained and single stains were used for establishing compensation and gates, and only live cells (DAPI negative) were analyzed.

Muscle DNA Electrotransfer

Hspa1b or GFP expression plasmids were transferred into contralateral limbs of HSP72-KO and WT mice as previously described (12). Muscles were harvested after 14 days following electroporation.

Immunoprecipitation and Immunoblot Analysis

Mouse tissues and cell cultures for immunoblotting were homogenized in RIPA lysis buffer containing protease and phosphatase inhibitors before being clarified and resolved by SDS-PAGE. Proteins for immunoprecipitations were solubilized in RIPA containing deoxycholate, 1% glycerol, and protease inhibitors by rotation at 4°C for 1 h, then cell debris were pelleted for 10 min at 5,000*g*. Total protein was measured, and 500 μg of sample was incubated with antibody (Mfn2, V5, HA, Parkin-4211) overnight then immobilized on protein-G agarose beads (Santa Cruz) for 2 h at 4°C prior to washing 3× in RIPA buffer. Proteins were resolved by SDS-PAGE. All samples for Western blotting were transferred to polyvinylidene fluoride membranes and probed with the following antibodies: HSP72 (Stressgen), glyceraldehyde-3-phosphate dehydrogenase (Millipore), p62 (ProGen), phosphatase and tensin homolog–induced putative kinase 1 (PINK1; Cayman Chemicals), DJ-1/Park7 (R&D Systems), Mfn2 (Abcam), porin/voltage-dependent anion channel (MitoSciences), Ubiquitin-FK2 (Enzo Life Sciences), HA-mouse (Covance), V5 (Invitrogen), DNAJB2 (Protein Tech Group), and cABL (BD Pharmingen). The following antibodies were all from Cell Signaling Technologies: p^{Ser473}-Akt (#9271), Parkin (#2132 & #4211), pan-actin, LC3B, Beclin1, LAMP1, HSP60, HSP90, and HA-rabbit. Densitometric analyses were performed using BioRad Chemidoc Quantity One image software.

Muscle Lipid Intermediates and Lipidomics Analyses

Lipids were extracted from the quadriceps muscle (n = 6 per genotype) by the Folch method (19). Triacylglycerol, diacylglycerol, and ceramides were extracted and quantified as previously described (19–21). Lipidomic analyses were performed by the Baker IDI Lipidomics Core on quadriceps samples homogenized in 300 μl PBS buffer, pH 7.47 according to previous methods, with modifications (22).

RNA Extraction, cDNA, and Quantitative RT-PCR

RNA from tissues and cells was extracted using RNeasy columns as per manufacturer's instructions (Qiagen). cDNA was synthesized from 1 μg of total RNA using SuperScript II as per manufacturer's instructions (Invitrogen). qPCR was performed on 20 ng cDNA on a BioRad MyiQ PCR Detection System using SyBR Green chemistry and analyzed using iQ5 Software (BioRad version 2.1) as previously described (10).

Statistics

Values presented are expressed as means ± SEM. Statistical analyses were performed using Student t tests as well as one- and two-way ANOVA with Tukey's post hoc comparison for identification of significance within and between groups where appropriate (SPSS graduate pack, Chicago, IL). Significance was set a priori at $P < 0.05$.

RESULTS

HSP72-KO Promotes an Insulin Resistance–Obesity Phenotype in Male Mice

Immunoblotting confirmed HSP72 protein was absent in glucoregulatory tissues harvested from male HSP72-KO mice compared with WT under both basal and heat shock conditions (Fig. 1*A*). Total body weight and gonadal fat pad mass were increased in HSP72-KO mice compared with WT despite consumption of a normal chow diet and no difference in ambulatory movement (Table 1). Basal glucose, leptin, resistin, and insulin levels were elevated, and adiponectin levels were reduced in plasma from HSP72-KO versus WT mice (Table 1). At ~24 weeks of age, we performed GTTs and, following intraperitoneal injection of dextrose, the glucose excursion for HSP72-KO mice was elevated compared with WT (Fig. 1*B*) (area under the curve P = 0.005), indicating impaired glucose tolerance in normal chow–fed HSP72-KO mice. No difference in plasma insulin was detected at 15 min following intraperitoneal dextrose injection (Table 1), a finding consistent with peripheral insulin resistance in the absence of pancreatic insufficiency. Euglycemic-hyperinsulinemic clamp studies were performed on weight-matched mice to quantify the impact of HSP72 deletion on insulin sensitivity. During steady-state clamp conditions, circulating glucose and insulin levels were identical between the genotypes (P = 0.57 and 0.87, respectively). The rate of exogenous glucose infusion required to maintain euglycemia was reduced by 33% (P = 0.007) in HSP72-KO mice compared with WT (Table 1), consistent with peripheral insulin resistance also observed during GTT. The insulin-stimulated glucose disposal, predominantly reflecting skeletal muscle insulin sensitivity, was reduced by 42% (P = 0.01) (Fig. 1*C*) in normal chow–fed HSP72-KO mice along with mild hepatic insulin resistance (Fig. 1*D*) compared with WT. In a separate cohort of animals 3 months of age, soleus muscles were stimulated ex vivo with a physiological insulin dose (60 μU/mL), and consistent with glucose clamp studies, insulin-stimulated muscle glucose uptake was reduced by 81% (P = 0.03) in HSP72-KO versus WT (Fig. 1*E*). Akt^{Ser473} phosphorylation paralleled the reduction in glucose uptake seen in KO muscle during insulin stimulation (Fig. 1*F*). Impaired insulin action could not be explained by a defect in myogenesis, Hsf1, or HSP90 expression, GLUT4 expression or total GLUT4 protein (Supplementary Fig. 1*A*–*E*).

Fatty acid oxidation was reduced (Fig. 1*G*), and fatty acid esterification (Fig. 1*H*) was elevated in HSP72-KO muscle versus WT, a finding consistent with a 28% reduction in AMPK activity (Fig. 1*I*) (P = 0.001), a 33% reduction β-hydroxyacyl CoA dehydrogenase activity (P = 0.035) (Supplementary Fig. 2*A*), and intramuscular accumulation of diacylglycerol and triacylglycerol (Fig. 1*J* and Supplementary Fig. 3). No difference in citrate synthase

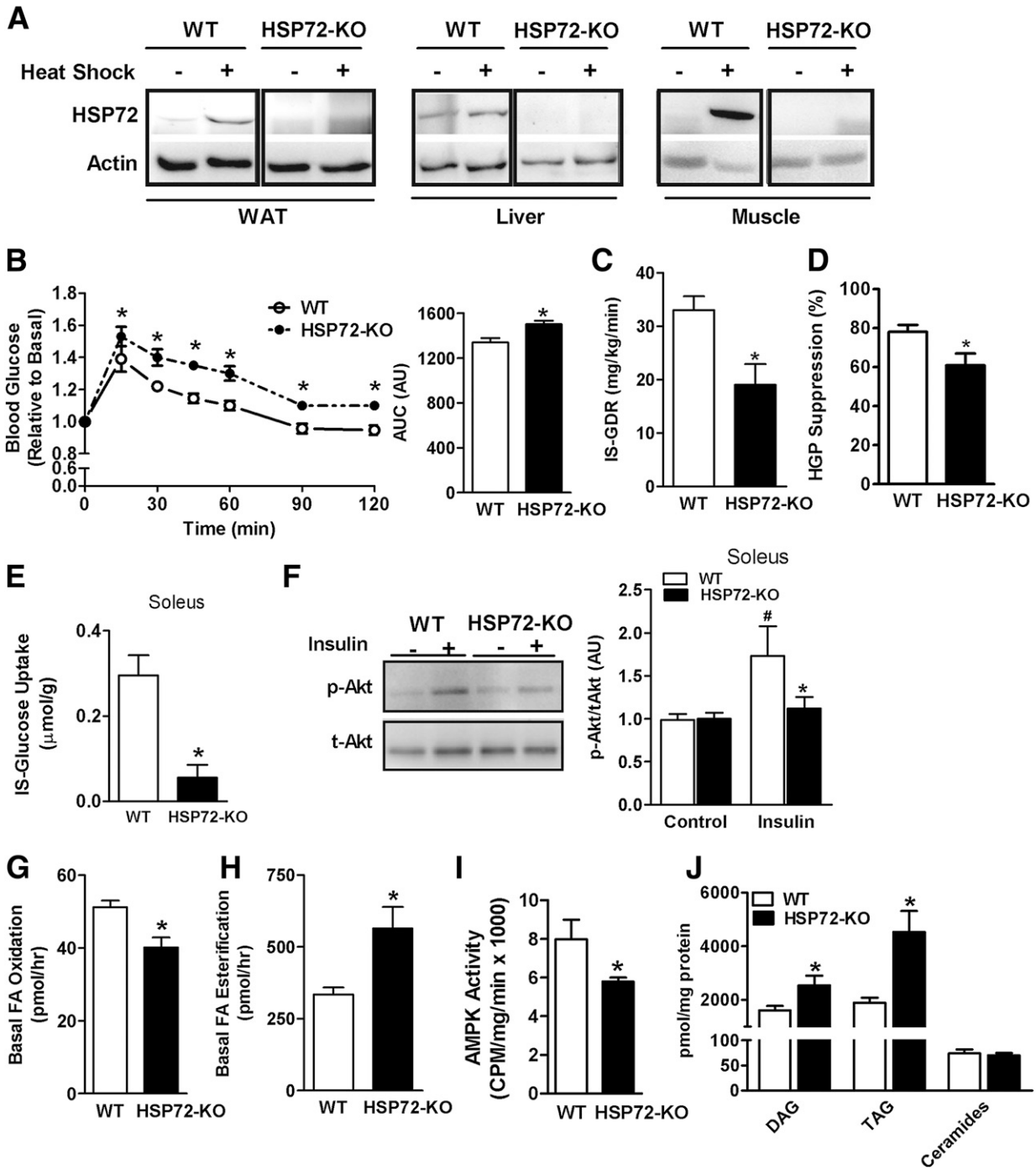

Figure 1—HSP72-KO promotes glucose intolerance and insulin resistance in male mice. *A*: Immunoblot analyses performed on gluco-regulatory tissues (white adipose tissue, liver, and muscle) confirms deletion of HSP72 in HSP72-KO tissues under basal and heat shock conditions. *B*: Glucose tolerance is impaired in KO mice (closed circles, dotted line) compared with WT (open circles, solid line; n = 10 mice/genotype). Hyperinsulinemic-euglycemic clamp studies show skeletal muscle and hepatic insulin resistance in HSP72-KO mice (closed bars; n = 8) as (*C*) insulin-stimulated glucose disposal rate and (*D*) hepatic glucose production (HGP) percentage suppression was significantly reduced compared with WT (open bars; n = 7 mice). *E*: Studies in isolated skeletal muscle (soleus) show impaired insulin-stimulated glucose uptake (n = 8 mice/genotype) and (*F*) reduced insulin-stimulated phosphorylation of Akt in HSP72-KO (closed bars) versus WT (open bars). *G*: Fatty acid oxidation was reduced, and (*H*) fatty acid esterification increased in isolated soleus muscles from HSP72-KO (closed bars) compared with WT (open bars) mice (n = 6/genotype). *I*: AMPK activity in quadriceps from WT and HSP72-KO mice (n = 6 mice/genotype). *J*: Diacylglycerol and triacylglycerol levels were elevated significantly in muscle from HSP72-KO (closed bars) versus WT (open bars; n = 6 mice/genotype) as measured by mass spectrometry. Values are expressed as means ± SEM. *, significance, $P < 0.05$, between genotypes; #, significance, $P < 0.05$, within genotype, between treatments. WAT, white adipose tissue; AUC, area under the curve; DAG, diacylglycerol; FA, fatty acid; HGP, hepatic glucose production; IS, insulin-stimulated; IS-GDR, insulin-stimulated glucose disposal rate; TAG, triacylglycerol; WAT, white adipose tissue.

activity, expression of cytochrome C oxidase subunits 2 and 3, or protein levels of electron transport chain subunits II–V were detected between the genotypes (Supplementary Fig. 2*B–D*).

HSP72-KD Impairs Insulin Action and Fatty Acid Handling in Myocytes

To determine if metabolic dysfunction observed in HSP72-KO mice was due to an intrinsic defect in skeletal muscle or secondary to increased adiposity, primary myoblasts were isolated from WT and HSP72-KO quadriceps muscle from 2-month-old mice. As expected, HSP72 transcript and protein levels were markedly reduced in HSP72-KO primary myotubes under both basal and heat shock conditions (Fig. 2*A* and *B*). HSP72-KO cells showed defective insulin-stimulated glucose uptake (Fig. 2*C*) consistent with reductions in insulin-stimulated Akt^{Ser473}-phosphorylation compared with WT (Fig. 2*D*). Similar to findings observed in soleus muscle from HSP72-KO mice, primary HSP72-KO myotubes, also exhibited reduced fatty acid oxidation and increased fatty acid esterification (Fig. 2*E* and *F*). Additionally, oxygen consumption (basal and maximal respiration) rates were reduced in primary myotubes from HSP72-KO mice compared with those from WT mice (Fig. 2*G*).

To validate these findings in an additional culture model, we generated C2C12 myotubes with HSP72-stable KD using lentiviral-mediated shRNA delivery compared with control scrambled shRNA cells (Fig. 2*H*). Fatty acid oxidation and esterification and cellular oxygen consumption at basal and during maximal stimulation in HSP72-KD C2C12 recapitulated findings for primary HSP72-KO myotubes relative to WT control (Fig. 2*I–K*). Impaired oxidative function tracked with cellular reactive oxygen species release as basal superoxide and H_2O_2 production were elevated in HSP72-KD myotubes compared with control scrambled (Fig. 2*L* and *M*).

HSP72 Is Critical for Maintenance of Mitochondrial Morphology, Parkin Protein, and Autophagic Signaling

To investigate the relationship between HSP72 expression and mitochondrial health, we assessed morphological differences in muscle mitochondria between WT and HSP72-KO animals. Electron micrographs of soleus muscle from 3-month-old animals showed enlarged, dysmorphic, and often fused intermyofibrillar mitochondria (Fig. 3*A*). Subsarcolemmal mitochondria also showed irregular morphology and reduced density by visual inspection. Since the subsarcolemmal mitochondrial compartment comprises only 20% of the total pool, the difference in mitochondrial number was not detected by a surrogate index of total mitochondrial DNA (mtDNA) (Supplementary Fig. 4). Considering that organelle fusion is a conserved mechanism engaged during chronic cellular stress (e.g., nutrient deprivation) as a means to maintain ATP production, avoid mitophagy, improve tolerance of mtDNA mutations by diluting damaged mitochondrial contents across the mitochondrial network (23), we investigated the underpinnings of this mitochondrial hyperfusion phenotype.

Typically, depolarized mitochondria are eliminated by a targeted autophagic process, mitophagy (24). The committed step in targeting mitochondria for lysosomal degradation occurs via activation of the PINK1/Parkin pathway (24). Parkin, an E3 ubiquitin ligase, translocates from the cytosol to depolarized mitochondria where it ubiquitinates mitochondrial-associated proteins, including Mfn1 and Mfn2, thus preventing fusion by promoting organelle isolation and subsequent autophagolysosome formation (24). Strikingly, we found that Parkin protein levels were dramatically increased in all glucoregulatory tissues from HSP72-KO mice. Importantly, Parkin protein was elevated 12-fold ($P = 0.0001$) (Fig. 3*B*) in skeletal muscle of HSP72-KO versus WT as early as 2 months of age prior to the onset of metabolic dysfunction (Supplementary Fig. 5). Under standard basal conditions, Parkin is rapidly turned over in WT cells replete with HSP72 (Supplementary Fig. 6); however, we found a marked accumulation of muscle Parkin in the absence of HSP72 under fed basal conditions. Thus the relative abundance of Parkin in WT or control samples was often difficult to visualize compared with the markedly increased abundance in HSP72-KO muscle and KD cells. In comparison with the dramatic elevation in Parkin protein in muscle, only a modest increase in muscle *Park2* transcript was observed (twofold; $P = 0.02$) (Supplementary Fig. 7), suggesting an important role of HSP72 in Parkin protein turnover. We surmise that Parkin overexpression is not likely a secondary phenotype in response to other in vivo factors, but a direct effect of HSP72 deletion as primary myotubes from HSP72-KO mice, and C2C12 myotubes with HSP72-KD also exhibited markedly elevated Parkin protein levels (Fig. 3*C* and *D*). Moreover, the effect of HSP72 appears unique to Parkin, as we observed no change in transcript or protein expression of other *Park* family members associated with mitophagic signaling (*Park6*, PINK1 and *Park7*, DJ-1) (Supplementary Fig. 7*A–C*).

The majority of Parkin in WT primary myotubes formed complexes at ~100 kDa and was sensitive to MG132 (a specific proteasomal inhibitor that reduces the degradation of ubiquitin-conjugated proteins), Baf (a specific inhibitor of vacuolar-type H+-ATPase that prevents lysosomal acidification and disturbs the fusion between autophagosomes and lysosomes), and the mitophagy inducer CCCP (an inhibitor of oxidative phosphorylation by destroying the mitochondrial electrochemical gradient) (Fig. 3*C*). However, Parkin was observed in its native unmodified form (~50 kDa) in HSP72-KO primary myotubes, and in contrast to WT, Parkin levels were unaffected by MG132, Baf, or CCCP treatment (Fig. 3*C*).

In addition to altered Parkin protein, downstream autophagic signaling was also impaired in both C2C12 myotubes as well as skeletal muscle. Protein levels of p62 (functionally targets damaged proteins and organelles for autophagy) and LC3BI (18 kDa microtubule-associated protein light chain B1 is recruited and converted to LC3BII by proteolysis and lipidation, which correlates well with autophagosome formation) were elevated (Fig. 3*D*, lanes 1–3 vs. 7–9;

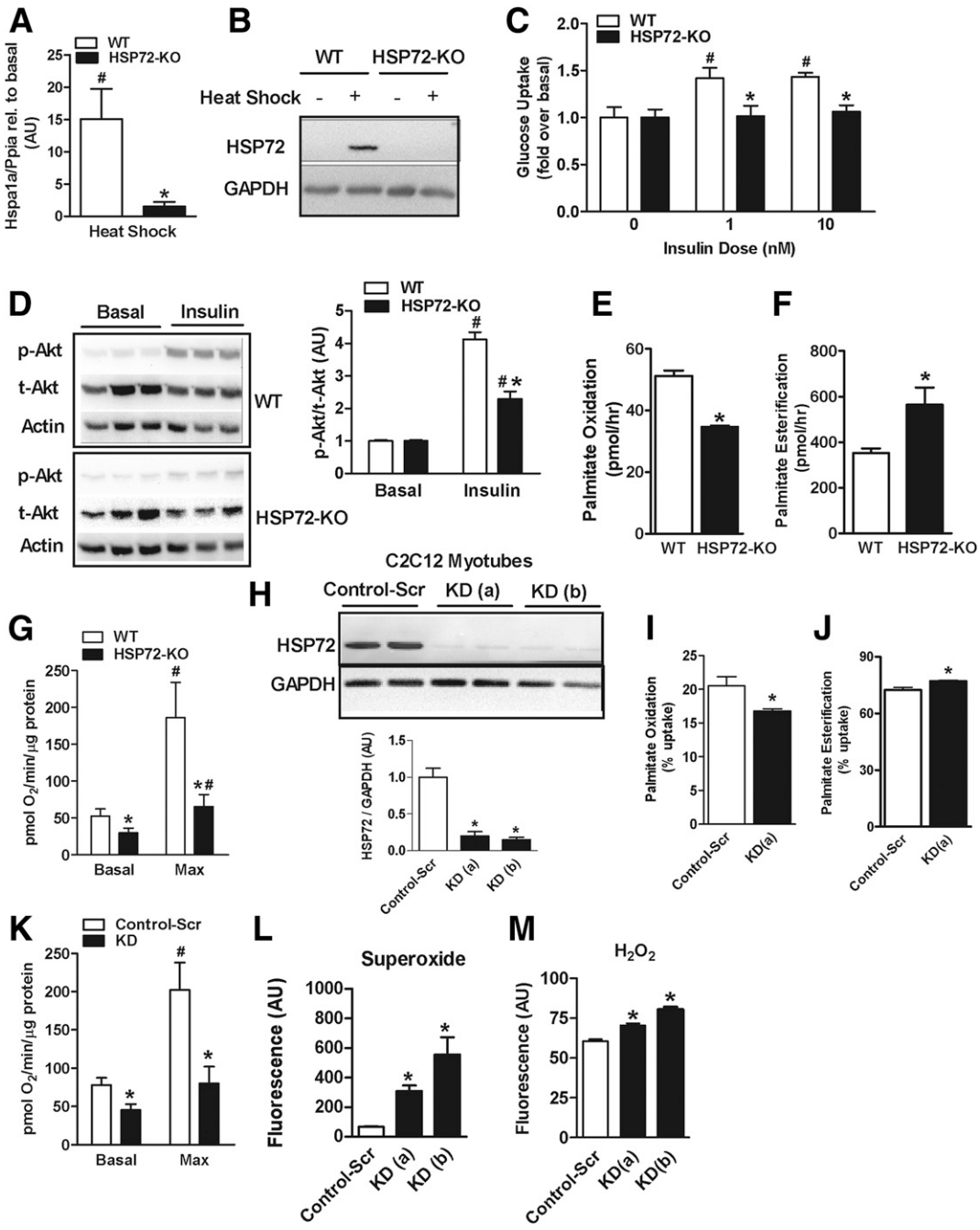

Figure 2—HSP72 deletion promotes insulin resistance and impaired fatty acid metabolism in myotubes. Primary myotubes from HSP72-KO mice (closed bars) show (*A*) reduced expression of *hspa1a* and (*B*) HSP72 protein after heat shock compared with cells from WT mice (open bars), measured by qPCR and immunoblotting, respectively. Impaired insulin action in HSP72-KO myotubes (closed bars) as shown by (*C*) reduced cellular glucose uptake and (*D*) impaired insulin-stimulated phosphorylation of Akt compared with WT (open bars; 5–8 observations/dose/genotype), as measured by densitometric analysis of immunoblotting ($n = 3$ representative samples run on same gel). Similar to findings in isolated soleus muscle, cultured myotubes from HSP72-KO mice show (*E*) reduced oxidation and (*F*) increased esterification of fatty acids. Consistent with impaired mitochondrial substrate handling, (*G*) real-time respirometry showed reduced basal and maximal O_2 consumption in HSP72-KO cells (closed bars), compared with WT (open bars; $n = 3 \times 12$ wells per genotype). *H*: HSP72 protein detected by immunoblotting in C2C12 cells infected with a lentivirus expressing either control scrambled shRNA (control scrambled) or two separate shRNAs against *Hspa1b*, KD(a), and KD(b). *I* and *J*: Impaired fatty acid oxidation and increased esterification in HSP72-KD cells treated with labeled palmitate. *K*: Similar to primary cells, real-time respirometry at basal and during maximal stimulation showed reduced O_2 consumption in C2C12 myotubes with HSP72-KD (closed bars) versus control scrambled (open bars). Increased reactive oxygen species production, (*L*) superoxide, and (*M*) H_2O_2, in both HSP72-KD cell lines (closed bars) compared with control scrambled (open bar), as measured by MitoSOX and DCF fluorescence, respectively ($n = 3$ in triplicate/condition). Values are expressed as means ± SEM. *, significance, $P < 0.05$, between genotypes; #, significance, $P < 0.05$, within genotype, between treatments. GAPDH, glyceraldehyde-3-phosphate dehydrogenase; Max, maximum; rel., relative; Scr, scrambled.

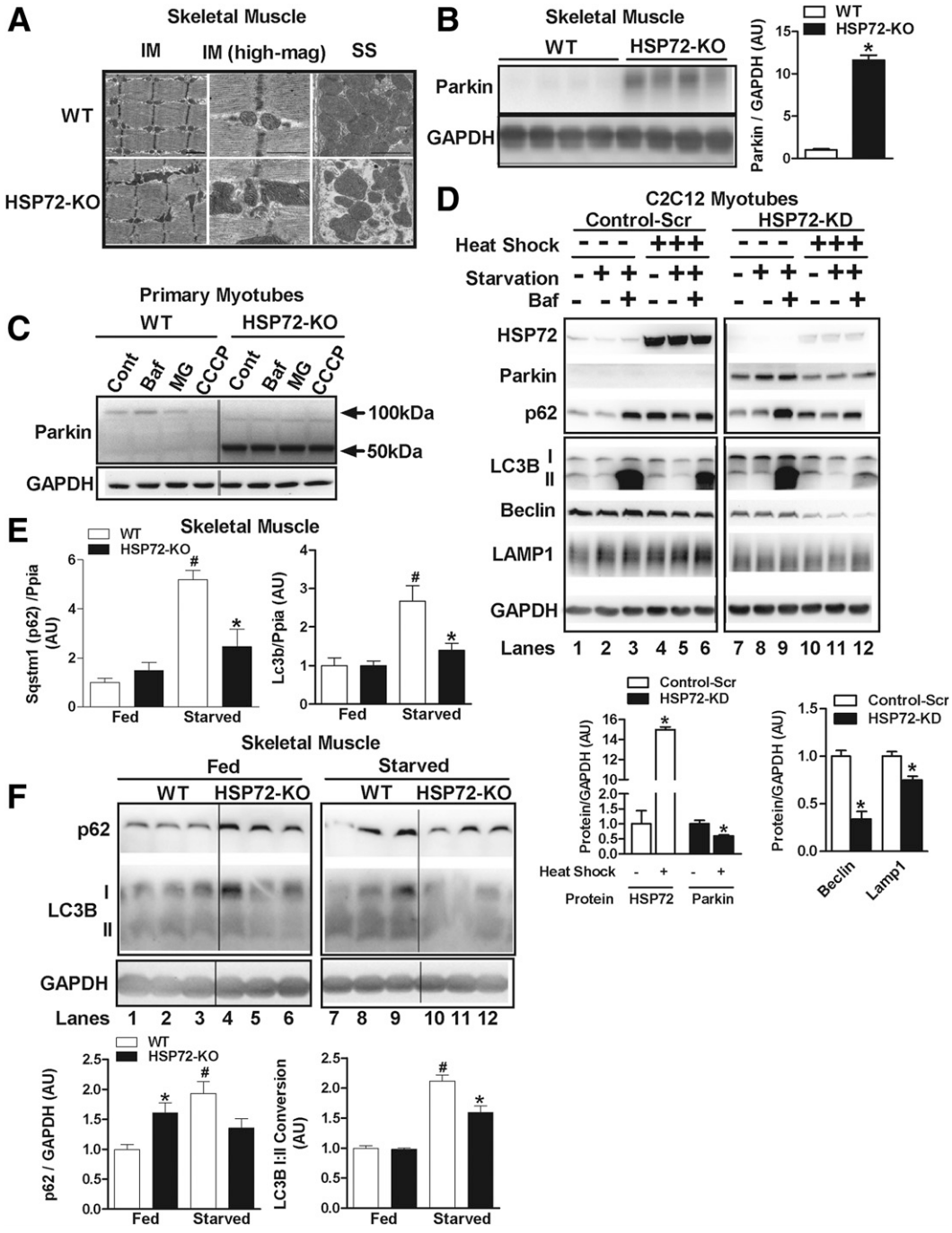

Figure 3—HSP72 is critical in the regulation of mitochondrial morphology, Parkin protein, and autophagic signaling in response to cellular stress. *A*: Electron micrographs of soleus muscle from WT (*top panels*) and KO (*bottom panels*) mice showing intermyofibrillar (*left panels*, low magnification; *middle panels*, high magnification) and subsarcolemmal (*right panels*) mitochondria (n = 4/genotype). *B*: Increased Parkin in quadriceps muscle from 9-month-old HSP72-KO versus WT mice shown by immunoblotting (n = 4 representative animals/genotype) and corresponding densitometry (n = 10/genotype). *C*: Immunoblotting performed on primary myotubes from mice shows increased Parkin protein at 50 kDa in HSP72-KO versus WT (immunoblot is from the same gel). *D*: Immunoblotting and densitometric analyses (*below*) performed on C2C12 myotubes show increased Parkin protein and impaired autophagic signaling, including increased p62 and LC3BI, and reduced Beclin and Lamp1 in HSP72-KD versus control scrambled cells (all immunoblots are from the same gel; n = 3–6/genotype). *E*: qPCR performed on muscle from WT and HSP72-KO mice under fed and starved (24 h) conditions shows blunted induction of p62 and LC3B in KO muscle following nutrient deprivation (n = 6/genotype). *F*: Immunoblotting of quadriceps muscle from fed and starved (24 h) WT and HSP72-KO mice (n = 3 representative samples/genotype/condition, *upper panel*; densitometric analyses, *lower panel*; n = 4–6 samples/genotype) show similar impairments in autophagic signaling as seen in cultured cells (all immunoblots are from the same gel and, in several instances, the membranes were cut, stripped, and reprobed to maximize the data obtained from each sample). Values are expressed as means ± SEM. *, significance, $P < 0.05$, between genotypes; #, significance, $P < 0.05$, within genotype, between treatments. Cont, control; GAPDH, glyceraldehyde-3-phosphate dehydrogenase; IM, intermyofibrillar; Scr, scrambled; SS, subsarcolemmal.

P = 0.045 and 0.01, respectively), while conversion to LC3BII (LC3BII:I) was diminished collectively reflecting reduced basal autophagic signaling in HSP72-KD versus control scrambled cells (Fig. 3*D*, lanes 1–3 vs. 7–9) and during heat shock (Fig. 3*D*, lanes 4–6 vs. 10–12) in both the absence and presence of the lysosomal inhibitor bafilomycin. A reduction in Beclin and Lamp1 protein in HSP72-KD versus control scrambled (P = 0.001 and 0.045, respectively) independent of treatment further supports this claim (Fig. 3*D*).

Although no difference in gene expression of Sqstm1 (p62) and Maplc3b (LC3B) between the genotypes in the fed state was detected (Fig. 3*E*), p62 and LC3BI protein levels were elevated in HSP72-KO muscle compared with WT (Fig. 3*F*, lanes 1–3 vs. 4–6). When comparing the conversion of LC3BI to BII between the genotypes, this was also blunted in the HSP72-KO muscle (Fig. 3*F*, lanes 1–3 vs. 4–6). During starvation, both Sqstm1 (p62) and Map1LC3B (LC3B) transcripts were markedly induced in WT; however, this induction was significantly blunted in HSP72-KO muscle (Fig. 3*E*). Despite reduced gene expression in muscle from HSP72-KO during starvation, p62 and LC3B-I protein levels were identical between the groups. Moreover, we observed reduced LC3BI to LC3BII conversion in HSP72-KO muscle compared with WT during starvation. Collectively, these data indicate a defect in autophagic signaling reflected by a reduction in the turnover and processing of p62 and LC3B in muscle devoid of HSP72.

HSP72, Parkin, and Insulin Action

To determine whether HSP72 is directly involved in Parkin protein regulation as suggested by findings in Fig. 3, we first used adenoviral re-expression of HSP72 in KO primary myotubes and found that partial restoration of HSP72 was sufficient to reduce Parkin protein levels by 24% (P = 0.03) after only 24 h (Fig. 4*A*; Supplementary Fig. 8). Similarly, we observed in C2C12 myotubes that heat shock induced a small increase in HSP72 protein in HSP72-KD cells, and this was associated with a 40% reduction (P = 0.03) in Parkin protein (Fig. 3*D*, *right panel*, lanes 7–9 vs. 10–12). Next we induced HSP72 expression by DNA electroporation into soleus muscle of HSP72-KO animals. Surprisingly, partial restoration of HSP72 expression in KO muscle was sufficient to reduce Parkin protein by ~50% versus soleus muscle electroporated with a plasmid to express GFP (Fig. 4*B*). In addition, we found that restoration of one *Hspa1* allele (heterozygous mice; gray bar) or muscle-specific transgenic overexpression of HSP72 in HSP72-KO markedly reduced muscle Parkin protein in 2-month-old mice by nearly 30% and 73%, respectively (Fig. 4*C*; P = 0.02) (Supplementary Fig. 9; P = 0.001). Collectively, these data suggest that HSP72 is a critical regulator of Parkin protein abundance.

Next we tested whether Parkin inactivation is linked with insulin resistance. Since the muscle phenotype of $Parkin^{-/-}$ mice is confounded by global Parkin deletion (25), we generated primary myotubes from these animals (Fig. 4*D*). Similar to HSP72-KO myotubes, maximal respiration was blunted in myotubes with Parkin inactivation (Fig. 4*E*), a finding consistent with observations in Parkin mutant *Drosophila* (26). Moreover, we found that basal glucose uptake was elevated; however, insulin-induced glucose uptake (Fig. 4*F*) and insulin signal transduction (Fig. 4*G*) were markedly reduced in Parkin-KO myotubes compared with WT. These findings strongly suggest that HSP72 is required for the regulation of Parkin protein levels and that Parkin functionality is directly linked with insulin action in muscle.

HSP72 Translocates to Depolarized Mitochondria and Is Required for Parkin Action

The aggregation of Parkin into nonfunctional clusters is thought to underlie Parkinson disease pathobiology (27). Thus we examined whether the inactivation and accumulation of Parkin in HSP72-KO muscle was due to Parkin aggregation and insolubility. We found that Parkin exists in the soluble fraction, suggesting that it does not form aggregates within muscle cells (Fig. 5*A*) and therefore is not likely to underlie the Parkin inactivation observed in this model.

Next we examined the cellular localization of Parkin using confocal microscopy. In the basal setting, Parkin was observed predominantly in the cytoplasm of myoblasts obtained from both WT and HSP72-KO mice (Fig. 5*B*). However, significantly more Parkin was observed in HSP72-KO than WT cells, a finding consistent with immunoblot analyses. Importantly, translocation of Parkin to depolarized mitochondria (CCCP treated) was impaired in HSP72-KO muscle cells (Fig. 5*B*). Specifically, in WT cells, CCCP induced mitochondrial depolarization and movement of Parkin from the cytosol to mitochondria (punctate staining); however, Parkin translocation was significantly blunted in HSP72-KO muscle cells (Fig. 5*B*). Furthermore, isolated mitochondria from WT myotubes contained more Parkin compared with HSP72-KO myotubes that showed no appreciable increase in Parkin following CCCP treatment (Fig. 5*C*). Moreover, Mfn2, typically ubiquitinated and targeted for proteasomal degradation by Parkin, was elevated in HSP72-KO myotubes compared with WT cells, a finding likely explained by reduced Parkin-mediated Mfn2 degradation (Fig. 5*C*).

Autoubiquitination can be used as a surrogate marker of Parkin activation. Immunoprecipitation studies showed that Parkin is ubiquitinated both basally and after CCCP treatment; however, the level of ubiquitination was significantly reduced in HSP72-KO compared with WT myotubes (Fig. 5*D*, *right panel*, lanes 5–6 vs. 7–8). Furthermore, basal Mfn2 protein levels in total lysates were markedly higher in HSP72-KO cells compared with control (Fig. 5*D*, *left panel*, lanes 1–2 vs. 3–4), a finding consistent with the mitochondrial hyperfusion phenotype. Considering this increase, the relative association and diminished subsequent turnover of Mfn2 in HSP72-KO compared with WT following CCCP treatment (Fig. 5*D*, *right*

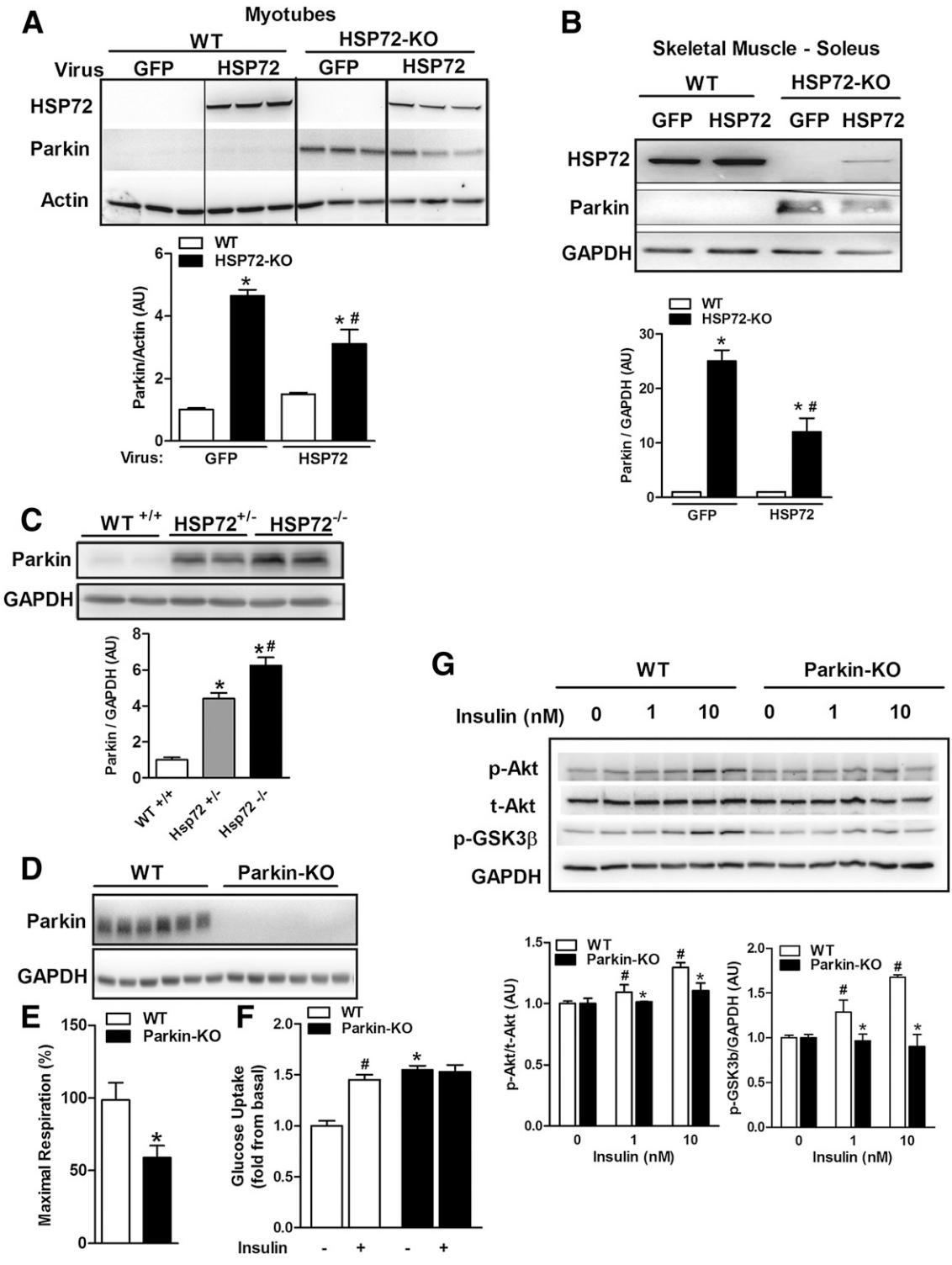

Figure 4—HSP72, Parkin, and insulin action. *A*: Representative immunoblots and densitometry for HSP72-KO myotubes infected with control empty virus or HSP72 adenovirus show reduction of Parkin protein following HSP72 reconstitution (n = 5 experiments/condition; n = 3 representative blots/condition). *B*: Immunoblots of Parkin and HSP72 protein from soleus muscle of WT and HSP72-KO mice (n = 3/genotype) electroporated with GFP (right leg) or HSP72 expression plasmid (left leg). *C*: Representative immunoblots (n = 2 /genotype) and densitometry (n = 10/per genotype) of Parkin from WT (open bars), HSP72$^{+/-}$ (gray bars), and HSP72$^{-/-}$ (closed bars) mice. *D*: Representative immunoblots of Parkin protein in primary myotubes from WT and Parkin-KO mice (n = 6/genotype). *E*: Real-time respirometry showing reduced maximal respiration in primary myotubes from Parkin-KO versus WT mice (n = 6/genotype). *F*: Impaired insulin-stimulated (10 nmol/L) glucose uptake and (*G*) insulin signaling (1 and 10 nmol/L) in Parkin-KO versus WT myotubes (n = 3 observations performed in duplicate; n = 2 representative blots/condition). Values are expressed as means ± SEM. *, significance, $P < 0.05$, between genotypes; #, significance, $P < 0.05$, within genotype, between treatments. GAPDH, glyceraldehyde-3-phosphate dehydrogenase.

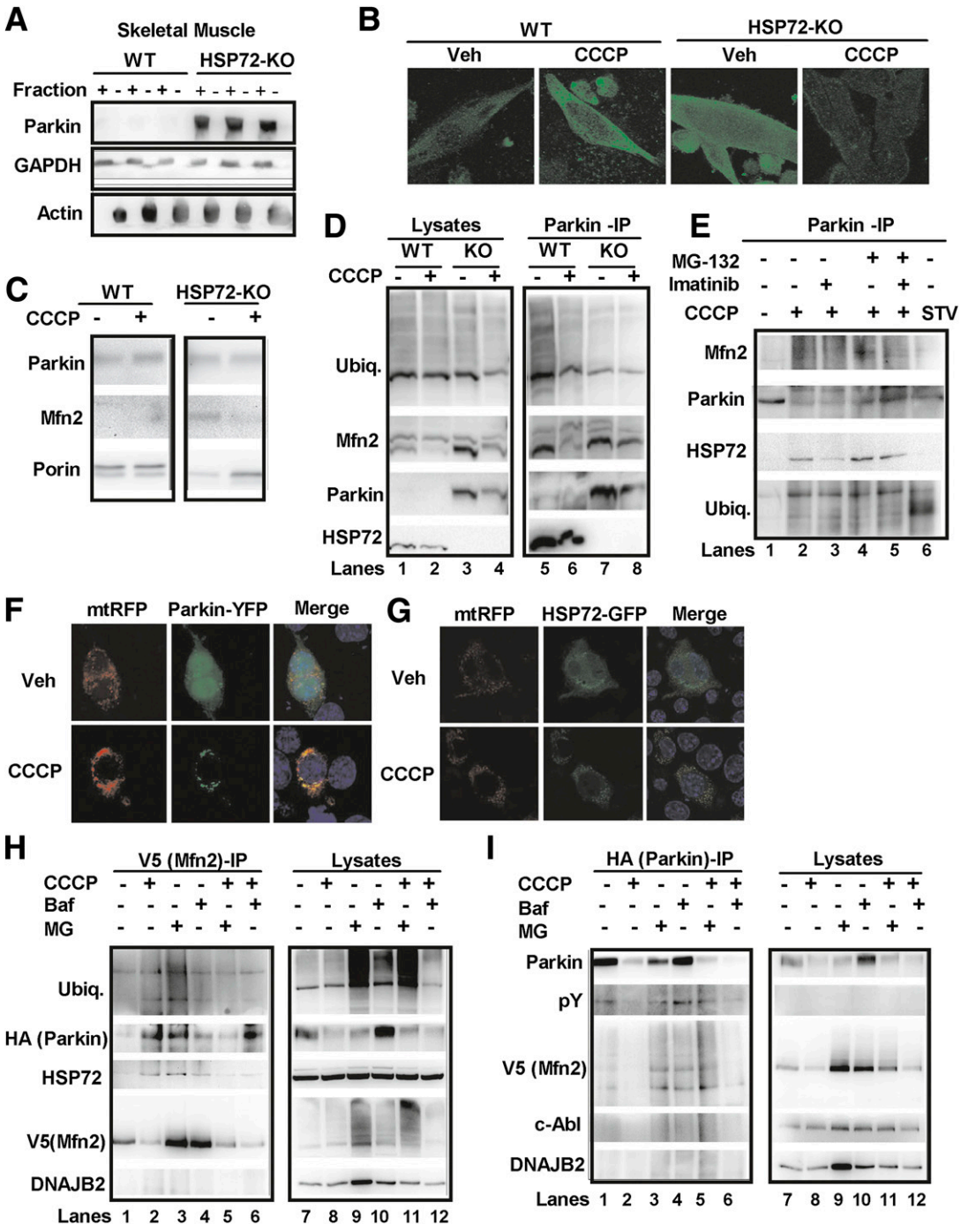

Figure 5—HSP72 translocates to damaged mitochondria and regulates Parkin-mediated mitophagic signaling. *A*: Immunoblotting for Parkin in soluble (+) and pellet (–) fractions from WT and HSP72-KO mouse quadriceps (n = 3/genotype) shows that Parkin resides in the soluble fraction in HSP72-KO muscle. *B*: Confocal images of myotubes (Parkin immunolabeled green) treated with vehicle (DMSO) or CCCP show defective Parkin translocation to mitochondria in HSP72-KO versus WT myotubes following CCCP treatment. Impaired Parkin translocation was confirmed by (*C*) immunoblotting of mitochondrial fractions isolated from WT and HSP72-KO myotubes treated with or without CCCP for 4 h. *D*: Immunoblots of cell lysates (*left panel*) and Parkin immunoprecipitation (*right panel*) in myotubes show altered Parkin ubiquitination and interaction between Mfn2 and Parkin in HSP72-KO versus WT primary myotubes in response to CCCP. These observations are supported by (*E*) immunoblotting in HEK293A cells transfected with Parkin and exposed to MG132, imatinib, CCCP, or starvation as indicated. *F*: Confocal images of N2a cells transfected with mtRFP and Parkin YFP or (*G*) mtRFP and HSP72 GFP and treated with vehicle (DMSO) or CCCP for 4 h (nuclei stained with DAPI). *H* and *I*: Immunoblots of HEK293A cell treated with or without CCCP, Baf, or MG132; (*H*) lysates and V5 immunoprecipitation following transfection with Parkin and V5 Mfn2 or (*I*) lysates and HA immunoprecipitation following transfection with HA Parkin and V5 Mfn2. Immunoblots contained in boxes are from the same gel, respectively. Reciprocal immunoprecipitation studies were performed in duplicate while all other studies were performed in triplicate. GAPDH, glyceraldehyde-3-phosphate dehydrogenase; IP, immunoprecipitation; MG, MG132; STV, starvation; Ubiq., ubiquitination; Veh, vehicle.

panel, lanes 5–6 vs. 7–8) supports our hypothesis of impaired Parkin activity in the context of HSP72 deficiency. Importantly, these data demonstrate for the first time in muscle cells that HSP72 complexes with Parkin and Mfn2 to orchestrate mitochondrial triage signaling.

To confirm the interaction between HSP72 and Parkin in a second cell type, we next performed similar immunoprecipitation studies in WT HEK293A cells. As predicted, after CCCP-induced mitochondrial depolarization, we observed increased interaction between Parkin, Mfn2, and HSP72. In contrast, this interaction of proteins was not observed in WT cells in an alternative cellular stress condition, starvation (Fig. 5*E*), when mitochondrial fusion is engaged to prevent the autophagic degradation of healthy organelles (28). These data suggest that HSP72 interaction with Parkin is only promoted in response to specific mitochondrial insult, e.g., alteration in membrane potential. Moreover, the interaction of Parkin with HSP72 and Mfn2 appeared to be tightly linked with the ubiquitination status of Parkin and Mfn2 (Fig. 5*E*), as CCCP-induced polyubiquitination of Parkin, whereas only Parkin monoubiquitination was detected during starvation (Fig. 5*E*).

Since an increased interaction between HSP72 and Parkin suggested possible comigration of these proteins to the same cellular compartment under specific organelle stress, e.g., CCCP-induced mitochondrial membrane depolarization, we next investigated the mitochondrial-specific targeting of these proteins by overexpressing fluorescently tagged HSP72 (GFP) and Parkin (YFP) in Neuro2a cells (N2a; an easily transfectable cell line expressing little to no endogenous HSP72 or Parkin and frequently used to assess autophagy by confocal microscopy). As shown previously, Parkin resides in the cytoplasm under basal conditions (DMSO) and translocates to mitochondria (RFP-labeled) after treatment with CCCP (4 h) (Fig. 5*F*). Under basal conditions, HSP72 also resides in the cytoplasm, and for the first time, we show in two separate cell systems (myotubes and N2a cells) that HSP72 translocates to mitochondria following treatment with CCCP (Fig. 5*G*). Furthermore, using a reciprocal immunoprecipitation approach in HEK293A cells, we confirm the interaction of HSP72 with Mfn2 and Parkin (Mfn2 immunoprecipitation and Parkin immunoprecipitation; Fig. 5*H* and *I*, respectively). Moreover, as shown previously (24), proteasomal inhibition using MG132 partially dampened CCCP-induced degradation of Mfn2 and Parkin; however, under basal conditions, Mfn2 and Parkin accumulated only during inhibition of lysosomal degradation in the presence of bafilomycin. These data reflect differential regulation of protein turnover based upon cellular status and protein localization (Fig. 5*H* and *I*). In contrast to Parkin and Mfn2, HSP72 is not degraded after CCCP treatment in HEK293A cells (Fig. 5*H*, *right panel*).

Finally, although others have suggested that DnaJB2/HSP40 and cABL interact with Parkin to control its folding and turnover in neuronal cells (14,29), no protein association was detected in muscle or HEK293A cells under basal conditions or following treatment with the cABL inhibitor imatinib (Fig. 5*H*, *I*, and *E*, respectively). Collectively, these data suggest that HSP72 is a cellular stress sensor that translocates to the site of mitochondrial damage where it interacts with both Parkin and Mfn2 to likely facilitate degradation of mitochondrial components via selective autophagy. We provide strong evidence for the conservation of this regulatory mechanism in three cell types: skeletal muscle, HEK293A cells, and N2a cells. Nevertheless, questions still remain regarding the timing and specific stress conditions in which these interactions occur and whether HSP72 mitochondrial translocation is an initiating step in this process.

HSP72 Is Critical for CCCP-Induced Parkin Action

Since the majority of studies presented above were performed over a 4-h period, the temporal order in which HSP72 and Parkin translocate to depolarized mitochondria in response to CCCP treatment was unknown. Thus confocal analyses were performed using the easily transfectable N2a cell system overexpressing fluorescently tagged HSP72 and Parkin. Surprisingly, HSP72 rapidly translocated to mitochondria beginning as early as 15 min following CCCP treatment (Fig. 6*A*). The entire cytosolic pool was observed at the mitochondrial membrane within 30 min and sustained presence of HSP72 was seen for up to 4 h (Fig. 6*A*, *top panels*). In contrast, Parkin remained in the cytoplasm up to 60 min after CCCP treatment, but by 4 h, the majority of cellular Parkin was observed in the same location as HSP72 (Fig. 6*A*, *bottom panels*). These observations were also supported by immunoblotting in a similar study conducted in isolated mitochondria from HEK293A, showing reduced cytoplasmic and increased mitochondrial-associated HSP72 at 30 min, whereas mitochondrial Parkin protein and subsequent degradation on Mfn2 was not observed until 1 h following CCCP treatment (Fig. 6*B*). These findings suggest that HSP72 translocates to depolarized mitochondria prior to the movement of molecular machinery necessary for the removal of mitochondria via selective autophagy, i.e., mitophagy. Thus it is reasonable to speculate that HSP72 may be sensitive to perturbations in mitochondrial membrane potential and be involved in facilitating early steps of mitophagic signaling.

To determine the specificity of the HSP72 response to mitochondrial stress, we used confocal microscopy to determine whether HSP72 translocation to mitochondria also occurred following rotenone (electron transport chain complex I inhibitor) and antimycin (cytochrome C reductase inhibitor) treatments. Neither compound induced the translocation of HSP72 or Parkin at 30 min; however, after 4 h, rotenone, but not antimycin, induced HSP72 movement to mitochondria (Fig. 6*D*). Considering that neither compound is known to induce mitophagy, as expected, Parkin remained dispersed in the cytoplasm

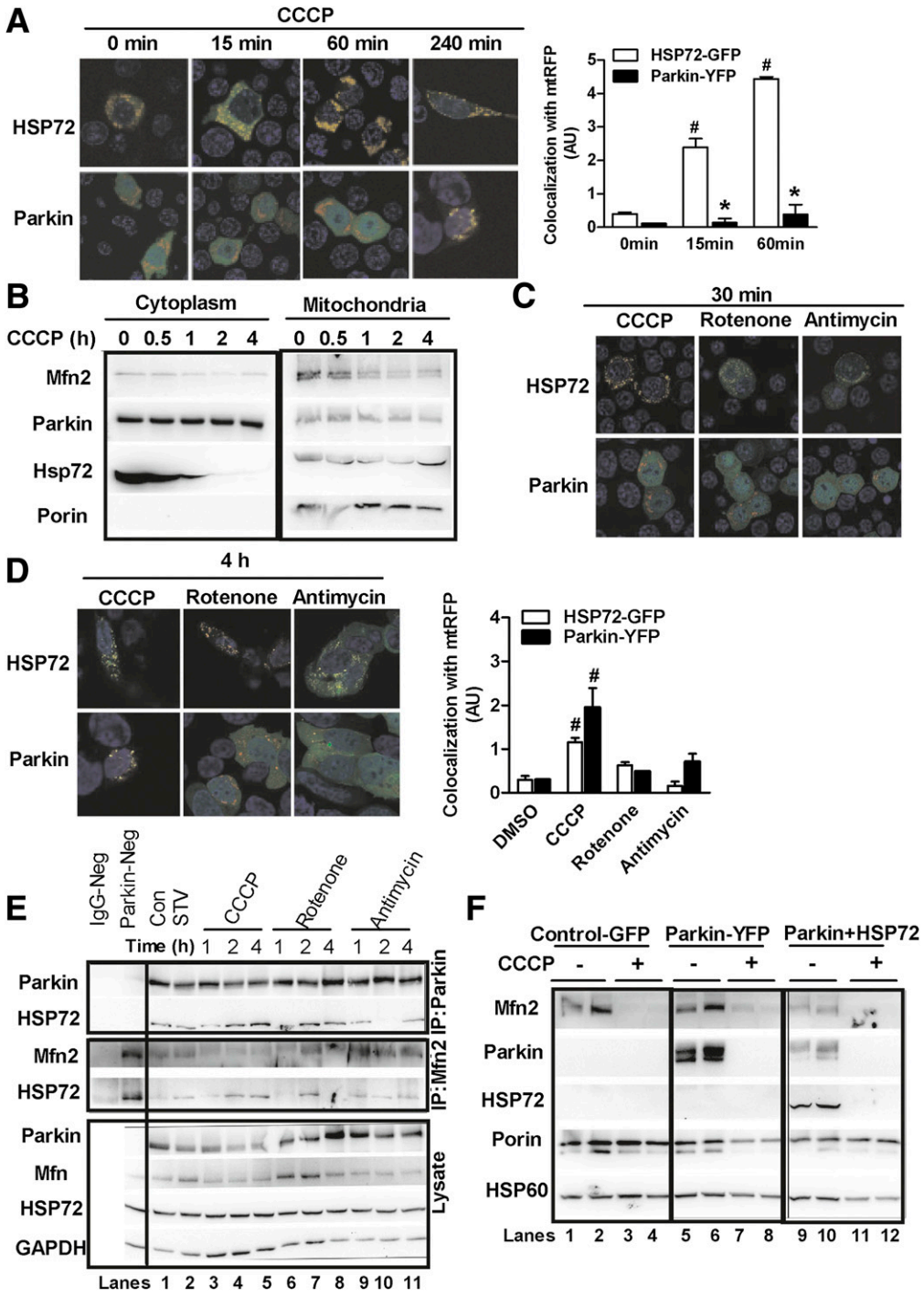

Figure 6—HSP72 is a mitochondrial stress sensor. *A*: Confocal images of HEK293A cells transfected with HSP72 GFP/mtRFP (*top panels*) and Parkin YFP/mtRFP (*bottom panels*) over a 120-min treatment with CCCP (nuclei stained with DAPI). *B*: Immunoblots performed on mitochondrial preps from HEK293A cells show the presence of mitochondrial Parkin and HSP72 concomitant with a reduction in the mitochondrial membrane-bound protein Mfn2 following 30-min/4-h CCCP treatment. *C*: Confocal micrographs of HEK293A cells transfected with HSP72 GFP (*top panels*) and Parkin YFP (*bottom panels*) following treatment with CCCP, rotenone, and antimycin for 0.5 h and (*D*) 4 h (nuclei stained with DAPI). *E*: Immunoblots of Parkin immunoprecipitation or Mfn2 immunoprecipitation (*top two panels*) or lysates (*bottom panels*) from HEK293A cells transfected with Parkin; treated with CCCP, rotenone, or antimycin for 1, 2, or 4 h; or starved for 4 h. *F*: Immunoblots of lysates from N2a cells transfected with GFP (*left panels*), Parkin YFP (*middle panels*), and Parkin + HSP72 (*right panels*) following treatment with vehicle (DMSO; CCCP [–]) or CCCP (+) for 12 h (immunoblots are from the same gel). Values are expressed as means ± SEM. *, significance, $P < 0.05$, between genotypes; #, significance, $P < 0.05$, within genotype, between treatments. *A*, *C*, and *D*: Performed twice in triplicate. *B*: Performed in duplicate in two independent cell lines. *E*: A replicative time course experiment. *F*: Performed twice in duplicate. Con, control; GAPDH, glyceraldehyde-3-phosphate dehydrogenase; IP, immunoprecipitation; Neg, negative; STV, starvation.

(30) (Fig. 6*C* and *D*). Congruent with confocal analyses, immunoprecipitation studies showed no increase in HSP72–Parkin association with Mfn2, and no degradation of the Parkin target Mfn2 following rotenone or antimycin treatment (Fig. 6*E*, lanes 6–11).

To demonstrate that HSP72 is required for Parkin action, we performed studies in N2a cells that lack detectable endogenous HSP72 and Parkin protein (Fig. 6*F*). Similar to previous findings, we show that HSP72 is critical for basal regulation of Parkin and Mfn2 protein levels (Fig. 6*F*, lanes 5–6 vs. 9–10). Using YFP-labeled Parkin, we demonstrated that CCCP failed to induce mitophagy in N2a cells in the absence of HSP72 and Parkin, as evidenced by a lack of reduction in porin or HSP60 levels after mitochondrial depolarization (Fig. 6*F*, *left panel*, lanes 1–2 vs. 3–4). However, when Parkin and HSP72 were introduced into this cell type, porin and HSP60 were diminished both at basal (Fig. 6*F*, lanes 1–2 and 5–6 vs. 9–10) and after CCCP treatment compared with GFP control (Fig. 6*F*, lanes 1–4 vs. 9–12), an observation consistent with enhanced mitochondrial turnover. Collectively, we found that a reduction in HSP72 promotes an increase and an inactivation of Parkin protein that is associated with alterations in mitochondrial quality and insulin resistance (Fig. 7).

DISCUSSION

The heat shock response is one of the most highly conserved processes from fly to man, and impairments in this protective mechanism are associated with increased cellular death (31–33) and reduced life span (2,3,34). The heat shock response is engaged during cellular stress to protect against proteotoxicity (35,36), and we have previously shown that HSP72, the stress-inducible protein chaperone, is reduced in skeletal muscle from obese and type 2 diabetic subjects (5,6). Conversely, we and others have also shown that upregulation of HSP72 by genetic, thermal stress, or pharmacologic means protects rodents from metabolic dysfunction induced by genetic or diet-induced obesity (6,37,38). Although clinical and experimental evidence suggests a strong relationship between HSP72 expression and glucose homeostasis, it was unknown whether reductions in HSP72 were causal of early metabolic dysfunction and insulin resistance. Furthermore, the critical targets of HSP72 that confer cellular protection remained incompletely understood.

Herein we provide compelling evidence to show that mice harboring a homozygous null mutation for *Hspa1a* and *Hspa1b* develop impaired glucose homeostasis, insulin resistance, and increased adiposity with age. Muscles from these mice accumulate bioactive lipids likely resulting

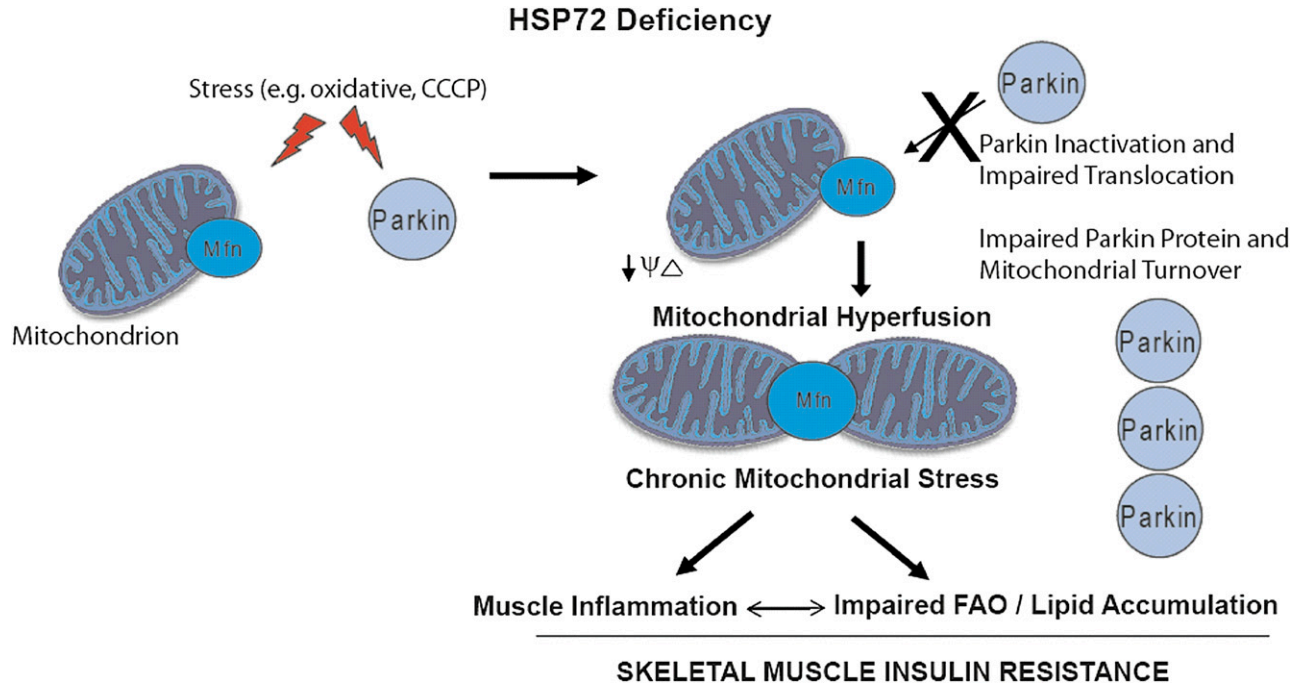

Figure 7—Proposed role of HSP72 in stress-induced mitophagy. Mitochondrial stress induces rapid movement of HSP72 to the mitochondria, where it interacts with Mfn2 on the outer mitochondrial membrane. At a later time point, Parkin translocates to the mitochondria and complexes with HSP72 and Mfn2. Herein we show that this interaction is specific to the mitochondrial insult. In the context of HSP72 deficiency, mitochondrial stress fails to induce Parkin translocation and interaction with mitochondrial membrane proteins. Parkin, in the absence of HSP72, is unable to ubiquitinate itself or its targets, and in consequence, cytosolic Parkin and mitochondrial Mfn2 protein levels become elevated, thus promoting the fusion and retention of unhealthy mitochondria to the network. We propose that this mechanism underlies the impairments in oxidative metabolism and marked insulin resistance phenotype observed in HSP72-KO animals. FAO, fatty acid oxidation.

from reduced fatty acid oxidation, and we postulate that this, in part, drives tissue inflammation. In addition, muscle cells lacking HSP72 have reduced oxygen consumption rates at basal and during maximal stimulation and increased mitochondrial reactive oxygen species production, an additional underpinning promoting cellular inflammation. Electron micrographs show a pronounced mitochondrial phenotype in HSP72-KO muscle that is characterized by enlarged, dysmorphic, and fused organelles with reduced density in the subsarcolemmal compartment. Healthy mitochondria typically elongate and fuse together during nutrient deprivation to avoid elimination by macroautophagy, although evidence also indicates tabulation and hyperfusion of mitochondria as a chronic compensatory adaptation to prolonged cellular stress (28,39,40), including loss of function in the PINK1/Parkin signaling pathway (41). Additionally, depolarized mitochondria can also fuse with healthy organelles when selective autophagy is impaired, and this mechanism serves a protective response to dilute damaged contents and maintain cellular energetics by functional complementation, a process thought to counteract cellular aging (42–44). Thus the chronic fusion phenotype we observe is likely a compensatory mechanism to help maintain cellular energetics, enhance DNA mutation tolerance with age, and prevent cellular apoptosis.

Recent work suggests that preservation of mitochondrial network health is achieved by the maintenance of paired fission–fusion events that accelerate the removal of damaged mitochondrial components by autophagy. This process, however, requires selectivity of fusion, especially under conditions of elevated mtDNA damage (45). The mitochondrial theory of aging portends that excessive production of reactive oxygen species induce mutations in mtDNA, and this precipitates reduced mitochondrial function, loss of bioenergetic capacity, and eventually disease pathology (46–51). This theory is consistent with impaired removal of dysfunctional mitochondria, and indeed skeletal muscle imbalances in fusion–fission dynamics have been associated with insulin resistance and metabolic dysfunction (52). Since no alteration in total mtDNA was detected, reduced oxygen consumption and elevated reactive oxygen species production in cells lacking HSP72 is consistent with retention of dysfunctional organelles, likely mediated by indiscriminate fusion and impaired mitophagy.

Thus the striking mitochondrial phenotype observed in HSP72-KO mice prompted us to investigate the integrity of mitophagic signaling, and considering previous reports suggesting HSPs as Parkin binding partners (53), we hypothesized that the retention of aged, damaged mitochondria could be due, in part, to impaired Parkin signaling. Interestingly, we found that HSP72 translocates to depolarized mitochondria within 15 min following CCCP treatment, even prior to the movement of Parkin. In the absence of HSP72, Parkin translocation to depolarized mitochondria was significantly diminished, and Mfn2, HSP60, and porin levels were maintained compared with control cells, findings consistent with the cellular retention of damaged mitochondria. Importantly, ectopic expression of HSP72 in N2a cells promoted CCCP-induced movement of Parkin to depolarized mitochondria concomitant with a reduction in the abundance of the Parkin target Mfn and mitochondrial markers porin and HSP60. These data suggest that HSP72 is a pivotal regulator of the Parkin–Mfn axis essential for mitochondrial quality control, although alternative E3 ligases and scaffolding proteins could also be engaged in the absence of Parkin in a cell type- and stress-specific manner.

It is important to note that the observed phenotype of the HSP72-KO mice phenocopies *Drosophila* lacking Parkin (7). Mitochondria from flight muscles of *Parkin*$^{-/-}$ flies appeared dysmorphic and were dysfunctional with impaired oxidative phosphorylation capacity and increased reactive oxygen species production. Similar to our findings in HSP72-KO mice, the mitochondrial defects in Parkin$^{-/-}$ flies preceded the muscle degeneration and both could be ameliorated by reducing oxidative stress. Although mice with homozygous null mutation of *Park2* (Parkin) show a less robust degeneration phenotype compared with *Drosophila* (54,55), *Parkin*$^{-/-}$ mice were more susceptible to environmental and inflammation-induced neural degeneration than WT littermates (56). Herein, we show for the first time that Parkin inactivation induces insulin resistance in primary myotubes, a finding with clinical implications linking impaired mitophagy with a central defining feature of the metabolic syndrome and type 2 diabetes.

Clearly maintenance of elemental processes, including preservation of protein and organelle quality, is critical for cellular health. Whether impaired macroautophagy and microautophagy are causal or consequence of insulin resistance remains unclear. Based upon our collective work, we provide strong evidence supporting a critical role for HSP72 in cellular stress sensing and Parkin action. Importantly, similar to our previous observations in human subjects (5,6), reduced HSP72 levels are associated with increased adiposity and impaired insulin action, whereas upregulation of HSP72 by chronic exercise, genetic overexpression, or pharmacological stimulation is protective against obesity and insulin resistance. Thus our work provides the important preclinical foundation to suggest that targeted therapies aimed at increasing muscle HSP72 may provide health benefit by ameliorating cellular oxidative damage, tissue inflammation, and insulin resistance, all underlying features of the metabolic syndrome and type 2 diabetes.

Acknowledgments. The authors appreciate the generosity of and informative discussions with Ming Guo (UCLA), David Chan (California Institute of Technology), Alexander Van der Bliek (UCLA), and Peter Tontonoz (UCLA). The authors thank the Advanced Light Microscopy/Spectroscopy facility at the California NanoSystems Institute at UCLA for assistance with confocal microscopy studies and Sirus Kohan of the UCLA Brain Research Institute for assistance with

electron microscopy studies on mouse muscle. Additional assistance was provided by Thomas Vallim and Peter Edwards (V5 and HA Gateway N-term plasmids); Erik Anderson and Douglas Black (Neuro2A cells); Steve Bensinger and Tammy Phung (assistance with flow cytometry analyses); Peter Meikle (Baker IDI Lipidomics Core); and Anna Calkin, Rima Boyadjian, and Peter Tontonoz (ubiquitination analyses and plasma adipokines were performed by the University of California, San Diego–UCLA DRC Inflammation Core).

Funding. This work was supported in part by the National Institutes of Health DK-078760 and University of California, San Diego–UCLA DRC Mouse Phenotyping Core DK-063491 to A.L.H. and by the National Health and Medical Research Council of Australia (project grant 1004441) to M.A.F. B.G.D. was supported by an Australian National Health and Medical Research Council Overseas Biomedical Training Fellowship (526693) and UCLA Jonsson Comprehensive Cancer Center Postdoctoral Research Fellowship. V.R. was supported by a postdoctoral fellowship from the Instituto de Salud Carlos III (Ministerio de Ciencia e Innovacion, Spain). D.C.H. was supported by a National Heart Foundation Biomedical Postdoctoral Fellowship and a Skip Martin Postdoctoral Fellowship from the Australian Diabetes Society. L.V. and K.R. are supported in part by the National Institutes of Health (HL28481), and the Seahorse XF24 Instrument is supported by a shared instrument grant from the National Institutes of Health National Center for Research Resources (S10RR026744). M.A.F. is a Senior Principal Research Fellow of the National Health and Medical Research Council of Australia.

Duality of Interest. M.A.F. is a consultant for N-Gene Biotechnology. No other potential conflicts of interest relevant to this article were reported.

Author Contributions. B.G.D. designed and carried out many of the in vitro and ex vivo experiments, conducted in vitro confocal microscopy and expression analyses, performed animal and tissues studies, and wrote the initial manuscript. V.R. assisted in conducting in vitro confocal microscopy and expression analyses and conducted oxygen consumption studies in myotubes. J.A.L. and Z.Z. assisted in conducting in vitro confocal microscopy and expression analyses. D.C.H. assisted in performing in vivo phenotyping of the HSP72-KO mice and contributed to the final drafting of the manuscript. J.P., T.S., P.D., and D.S. maintained the breeding colony and assisted in performing animal and tissues studies. L.V. assisted in conducting oxygen consumption studies in myotubes. J.W. provided advice and technical consultation and contributed to the final drafting of the manuscript. K.R. assisted in conducting oxygen consumption studies in myotubes and contributed to the final drafting of the manuscript. M.A.F. provided advice and technical consultation and contributed to the final drafting of the manuscript. A.L.H. performed in vivo phenotyping of the HSP72-KO mice, performed animal and tissues studies, supervised the project, and wrote the initial manuscript. A.L.H. is the guarantor of this work and, as such, had full access to all the data in the study and takes responsibility for the integrity of the data and the accuracy of the data analysis.

References

1. Balch WE, Morimoto RI, Dillin A, Kelly JW. Adapting proteostasis for disease intervention. Science 2008;319:916–919

2. Morley JF, Morimoto RI. Regulation of longevity in Caenorhabditis elegans by heat shock factor and molecular chaperones. Mol Biol Cell 2004;15:657–664

3. Hsu AL, Murphy CT, Kenyon C. Regulation of aging and age-related disease by DAF-16 and heat-shock factor. Science 2003;300:1142–1145

4. Febbraio MA, Koukoulas I. HSP72 gene expression progressively increases in human skeletal muscle during prolonged, exhaustive exercise. J Appl Physiol (1985) 2000;89:1055–1060

5. Bruce CR, Carey AL, Hawley JA, Febbraio MA. Intramuscular heat shock protein 72 and heme oxygenase-1 mRNA are reduced in patients with type 2 diabetes: evidence that insulin resistance is associated with a disturbed antioxidant defense mechanism. Diabetes 2003;52:2338–2345

6. Chung J, Nguyen AK, Henstridge DC, et al. HSP72 protects against obesity-induced insulin resistance. Proc Natl Acad Sci U S A 2008;105:1739–1744

7. Deng H, Dodson MW, Huang H, Guo M. The Parkinson's disease genes pink1 and parkin promote mitochondrial fission and/or inhibit fusion in Drosophila. Proc Natl Acad Sci U S A 2008;105:14503–14508

8. Hevener AL, Olefsky JM, Reichart D, et al. Macrophage PPAR gamma is required for normal skeletal muscle and hepatic insulin sensitivity and full antidiabetic effects of thiazolidinediones. J Clin Invest 2007;117:1658–1669

9. Hevener AL, He W, Barak Y, et al. Muscle-specific Pparg deletion causes insulin resistance. Nat Med 2003;9:1491–1497

10. Ribas V, Drew BG, Le JA, et al. Myeloid-specific estrogen receptor alpha deficiency impairs metabolic homeostasis and accelerates atherosclerotic lesion development. Proc Natl Acad Sci U S A 2011;108:16457–16462

11. Jørgensen SB, Wojtaszewski JF, Viollet B, et al. Effects of alpha-AMPK knockout on exercise-induced gene activation in mouse skeletal muscle. FASEB J 2005;19:1146–1148

12. Bruce CR, Hoy AJ, Turner N, et al. Overexpression of carnitine palmitoyltransferase-1 in skeletal muscle is sufficient to enhance fatty acid oxidation and improve high-fat diet-induced insulin resistance. Diabetes 2009;58:550–558

13. Henstridge DC, Drew BG, Formosa MF, et al. The effect of the nitric oxide donor sodium nitroprusside on glucose uptake in human primary skeletal muscle cells. Nitric Oxide 2009;21:126–131

14. Ko HS, Lee Y, Shin JH, et al. Phosphorylation by the c-Abl protein tyrosine kinase inhibits parkin's ubiquitination and protective function. Proc Natl Acad Sci U S A 2010;107:16691–16696

15. McCurdy CE, Cartee GD. Akt2 is essential for the full effect of calorie restriction on insulin-stimulated glucose uptake in skeletal muscle. Diabetes 2005;54:1349–1356

16. Bolte S, Cordelières FP. A guided tour into subcellular colocalization analysis in light microscopy. J Microsc 2006;224:213–232

17. Taylor SW, Fahy E, Zhang B, et al. Characterization of the human heart mitochondrial proteome. Nat Biotechnol 2003;21:281–286

18. Wang C, Tan JM, Ho MW, et al. Alterations in the solubility and intracellular localization of parkin by several familial Parkinson's disease-linked point mutations. J Neurochem 2005;93:422–431

19. Frayn KN, Maycock PF. Skeletal muscle triacylglycerol in the rat: methods for sampling and measurement, and studies of biological variability. J Lipid Res 1980;21:139–144

20. Preiss J, Loomis CR, Bishop WR, Stein R, Niedel JE, Bell RM. Quantitative measurement of sn-1,2-diacylglycerols present in platelets, hepatocytes, and ras- and sis-transformed normal rat kidney cells. J Biol Chem 1986;261:8597–8600

21. Allred JB, Guy DG. Determination of coenzyme A and acetyl CoA in tissue extracts. Anal Biochem 1969;29:293–299

22. Matthews VB, Allen TL, Risis S, et al. Interleukin-6-deficient mice develop hepatic inflammation and systemic insulin resistance. Diabetologia 2010;53:2431–2441

23. Chan DC. Fusion and fission: interlinked processes critical for mitochondrial health. Annu Rev Genet 2012;46:265–287

24. Chan DC. Mitochondria: dynamic organelles in disease, aging, and development. Cell 2006;125:1241–1252

25. Kim KY, Stevens MV, Akter MH, et al. Parkin is a lipid-responsive regulator of fat uptake in mice and mutant human cells. J Clin Invest 2011;121:3701–3712

26. Vincent A, Briggs L, Chatwin GF, et al. parkin-induced defects in neurophysiology and locomotion are generated by metabolic dysfunction and not oxidative stress. Hum Mol Genet 2012;21:1760–1769

27. Kitada T, Asakawa S, Hattori N, et al. Mutations in the parkin gene cause autosomal recessive juvenile parkinsonism. Nature 1998;392:605–608

28. Rambold AS, Kostelecky B, Lippincott-Schwartz J. Fuse or die: Shaping mitochondrial fate during starvation. Commun Integr Biol 2011;4:752–754

29. Rose JM, Novoselov SS, Robinson PA, Cheetham ME. Molecular chaperone-mediated rescue of mitophagy by a Parkin RING1 domain mutant. Hum Mol Genet 2011;20:16–27

30. Tanaka A, Cleland MM, Xu S, et al. Proteasome and p97 mediate mitophagy and degradation of mitofusins induced by Parkin. J Cell Biol 2010;191:1367–1380
31. Ben-Zvi A, Miller EA, Morimoto RI. Collapse of proteostasis represents an early molecular event in Caenorhabditis elegans aging. Proc Natl Acad Sci USA 2009;106:14914–14919
32. Morimoto RI. Proteotoxic stress and inducible chaperone networks in neurodegenerative disease and aging. Genes Dev 2008;22:1427–1438
33. Ritossa F. Discovery of the heat shock response. Cell Stress Chaperones 1996;1:97–98
34. Volovik Y, Maman M, Dubnikov T, et al. Temporal requirements of heat shock factor-1 for longevity assurance. Aging Cell 2012;11:491–499
35. Gidalevitz T, Prahlad V, Morimoto RI. The stress of protein misfolding: from single cells to multicellular organisms. Cold Spring Harb Perspect Biol 2011;3
36. Kikis EA, Gidalevitz T, Morimoto RI. Protein homeostasis in models of aging and age-related conformational disease. Adv Exp Med Biol 2010;694:138–159
37. Gupte AA, Bomhoff GL, Swerdlow RH, Geiger PC. Heat treatment improves glucose tolerance and prevents skeletal muscle insulin resistance in rats fed a high-fat diet. Diabetes 2009;58:567–578
38. Gupte AA, Bomhoff GL, Touchberry CD, Geiger PC. Acute heat treatment improves insulin-stimulated glucose uptake in aged skeletal muscle. J Appl Physiol (1985) 2011;110:451–457
39. Gomes LC, Di Benedetto G, Scorrano L. During autophagy mitochondria elongate, are spared from degradation and sustain cell viability. Nat Cell Biol 2011;13:589–598
40. Gomes LC, Scorrano L. Mitochondrial elongation during autophagy: a stereotypical response to survive in difficult times. Autophagy 2011;7:1251–1253
41. Poole AC, Thomas RE, Andrews LA, McBride HM, Whitworth AJ, Pallanck LJ. The PINK1/Parkin pathway regulates mitochondrial morphology. Proc Natl Acad Sci USA 2008;105:1638–1643
42. Chen H, Chan DC. Physiological functions of mitochondrial fusion. Ann N Y Acad Sci 2010;1201:21–25
43. Chen H, Vermulst M, Wang YE, et al. Mitochondrial fusion is required for mtDNA stability in skeletal muscle and tolerance of mtDNA mutations. Cell 2010;141:280–289
44. Peterson CM, Johannsen DL, Ravussin E. Skeletal muscle mitochondria and aging: a review. J Aging Res 2012;2012:194821
45. Mouli PK, Twig G, Shirihai OS. Frequency and selectivity of mitochondrial fusion are key to its quality maintenance function. Biophys J 2009;96:3509–3518
46. Harman D. Free-radical theory of aging. Increasing the functional life span. Ann N Y Acad Sci 1994;717:1–15
47. Wallace DC. Mitochondrial diseases in man and mouse. Science 1999;283:1482–1488
48. Linnane AW, Marzuki S, Ozawa T, Tanaka M. Mitochondrial DNA mutations as an important contributor to ageing and degenerative diseases. Lancet 1989;1:642–645
49. Miquel J, Economos AC, Fleming J, Johnson JE Jr. Mitochondrial role in cell aging. Exp Gerontol 1980;15:575–591
50. Stadtman ER, Berlett BS. Reactive oxygen-mediated protein oxidation in aging and disease. Chem Res Toxicol 1997;10:485–494
51. Balaban RS, Nemoto S, Finkel T. Mitochondria, oxidants, and aging. Cell 2005;120:483–495
52. Sebastián D, Hernández-Alvarez MI, Segalés J, et al. Mitofusin 2 (Mfn2) links mitochondrial and endoplasmic reticulum function with insulin signaling and is essential for normal glucose homeostasis. Proc Natl Acad Sci U S A 2012;109:5523–5528
53. Sarraf SA, Raman M, Guarani-Pereira V, et al. Landscape of the PARKIN-dependent ubiquitylome in response to mitochondrial depolarization. Nature 2013;496:372–376
54. Goldberg MS, Fleming SM, Palacino JJ, et al. Parkin-deficient mice exhibit nigrostriatal deficits but not loss of dopaminergic neurons. J Biol Chem 2003;278:43628–43635
55. Oyama G, Yoshimi K, Natori S, et al. Impaired in vivo dopamine release in parkin knockout mice. Brain Res 2010;1352:214–222
56. Frank-Cannon TC, Tran T, Ruhn KA, et al. Parkin deficiency increases vulnerability to inflammation-related nigral degeneration. J Neurosci 2008;28:10825–10834